ADVANCES IN ATMOSPHERIC SCIENCES, VOL. 35, JULY 2018, 826–838

• **Original Paper** •

Regional Characteristics of Typhoon-Induced Ocean Eddies in the East China Sea

Jianhong WANG*[1,2], Meiqi LI[1,5], X. San LIANG[1,2], Xing WANG[1], Feng XUE[4], Mo PENG[3], and Chunsheng MIAO[1]

[1]*Collaborative Innovation Center on Forecast and Evaluation of Meteorological Disasters/College of Atmospheric Science, Nanjing University of Information Science and Technology, Nanjing* 210044*, China*

[2]*School of Marine Sciences, Nanjing University of Information Science and Technology, Nanjing* 210044*, China*

[3]*Jiangsu Tidal Flat Research Center / Jiangsu Ocean Environment Forecast Center, Nanjing* 210000*, China*

[4]*National Meteorological Center of China Meteorological Administration, Beijing* 100081*, China*

[5]*Hebei Provincial Meteorological Service Center, Shijiazhuang* 050000*, China*

(Received 15 July 2017; revised 21 November 2017; accepted 19 December 2017)

ABSTRACT

The asymmetrical structure of typhoon-induced ocean eddies (TIOEs) in the East China Sea (including the Yellow Sea) and the accompanying air–sea interaction are studied using reanalysis products. Thirteen TIOEs are analyzed and divided into three groups with the *k*-prototype method: Group A with typhoons passing through the central Yellow Sea; Group B with typhoons re-entering the sea from the western Yellow Sea after landing on continental China; and Group C with typhoons occurring across the eastern Yellow Sea near to the Korean Peninsula. The study region is divided into three zones (Zones I, II and III) according to water depth and the Kuroshio position. The TIOEs in Group A are the strongest and could reverse part of the Kuroshio stream, while TIOEs in the other two groups are easily deformed by topography. The strong currents of the TIOEs impact on the latent heat flux distribution and upward transport, which facilitates the typhoon development. The strong divergence within the TIOEs favors an upwelling-induced cooling. A typical TIOE analysis shows that the intensity of the upwelling of TIOEs is proportional to the water depth, but its magnitude is weaker than the upwelling induced by the topography. In Zones I and II, the vertical dimensions of TIOEs and their strong currents are much less than the water depths. In shallow water Zone III, a reversed circulation appears in the lower layer. The strong currents can lead to a greater, faster, and deeper energy transfer downwards than at the center of TIOEs.

Key words: typhoon-induced ocean eddies, East China Sea, asymmetrical dynamic structure, kinetic energy transfer and evolution

Citation: Wang, J. H., M. Q. Li, X. S. Liang, X. Wang, F. Xue, M. Peng, and C. S. Miao, 2018: Regional characteristics of typhoon-induced ocean eddies in the East China Sea. *Adv. Atmos. Sci.*, **35**(7), 826–838, https://doi.org/10.1007/s00376-017-7173-4.

1. Introduction

The interaction between typhoons or tropical storm cyclones and the upper ocean is complicated. On the one hand, the wind stress of these strong rotating systems can generate oceanic eddies. On the other hand, the oceanic surface circulations impacted by these tropical rotating systems will redistribute the sea temperature and salinity, and hence affect the atmospheric systems above by sea surface thermodynamic and moisture fluxes. For brevity, "typhoon" is used in this paper to indicate the systems of typhoons and tropical storm cyclones, and the ocean eddies they cause are referred to as typhoon-induced ocean eddies (TIOEs). Obviously, air–sea interaction is pivotal in the study of typhoon and tropical storm genesis and maintenance.

Mesoscale ocean eddies usually have a horizontal scale of 50–500 km, a maximum vertical scale of 5 km, a life time of several days to more than 100 days, and a moving speed of only ~ 10 cm s^{-1} (Nencioli et al., 2010; Yang et al., 2013). So far, studies on mesoscale ocean eddies have been mostly based on statistics and are region specific (Ma et al., 2014; Yin, 2014; Qin et al., 2015). It is reported that ocean mesoscale eddies account for more than 80% of the total average kinetic energy of the ocean; they also play important roles in ocean energy redistribution and transport, and are crucial in forming the biological and chemical environment (Yang et al., 2010; Shang et al., 2013; Chen et al., 2013). As a particular class of mesoscale eddies with distinct generating mechanisms, TIOEs are remarkable because, in terms of spatial scale, the radii of TIOEs are larger than most mesoscale ocean eddies, and in terms of temporal scale they are relatively short-lived. More specifically, the mixing in the upper ocean is enhanced as a typhoon passes, and usu-

* Corresponding author: Jianhong WANG
Email: 1597706505@qq.com

ally cold water upwells from below (Leipper, 1967; Black, 1983; Shay, 2010; Zheng et al., 2010). Subsequently, the sea surface temperature (SST) cools and sea water salinity reduces (Monaldo et al., 1996; Wentz et al., 2000; Liu et al., 2007, 2014; Domingues et al., 2015). As a result, the surface mixed layer deepens (Emanuel, 1999; Lin, 2005; Nam et al., 2012), the sea surface height decreases, and the circulation enhances (Liu and Hu, 2009; Tsai et al., 2013; Sun et al., 2014). Compared to normal eddies, TIOEs are more intense, with a shorter life span, and hence have a stronger and more immediate impact on the distribution and variability of the ocean temperature, salinity, and energy transfer. In short, TIOEs are different from mesoscale ocean eddies in a general sense; they call for special attention, considering their roles in typhoon processes.

The present study focuses mainly on TIOEs in the East China Sea (including the Yellow Sea), which features many islands and complex terrain. The water depth changes from 80–100 m on the shelf to more than 1000 m east of Taiwan. Besides, a strong western boundary current, the Kuroshio, is directly involved in the circulation therein. Such a geometric and dynamic configuration may significantly affect the characteristics of TIOEs, making them different from the eddies in the open sea. In this study, we analyze the 13 TIOEs identified in the ECS during the 11 years from 2005 to 2015. We particularly focus on the structures and energy transfer processes underlying them via comparative analysis and dynamic diagnosis, in order to enhance our understanding of their characteristics and their roles in the ECS circulation.

2. Data and methods

2.1. *Data*

To investigate the ECS TIOEs, four kinds of datasets can be used: the sea surface height anomaly (SSHA) field retrieved by satellite altimeter (Yang et al., 2012; Li, 2015), in-situ data including those from Argo floats and buoys (Yang et al., 2010; Sun et al., 2012), reanalysis data, and numerical simulation products. For the SSHA, a calculation is needed to extract the TIOEs. The in-situ data are point-wise, so they do not reflect the overall features of a whole TIOE. The reanalysis data and products of models can provide simulated TIOEs based on modeled physical processes, the flow fields meet the wind pressure relation and ocean current relation laws, and can show the temporal and spatial features in detail. In this sense, reanalysis data and modeling products are better than satellite data for this purpose. Particularly, it has been reported that the Hybrid Coordinate Ocean Model (HYCOM) dataset (http://hycom.org/dataserver/) is a satisfactory choice (Tanajura et al., 2014; Zhang et al., 2014); it assimilates satellite altimeter data, and temperature and salinity profile data from the expendable bathythermograph (XBTs) Argo floats, and moorings, with a temporal resolution of 3 h before 2013, and daily afterward, at 40 levels, and a horizontal resolution of (1/12)°×(1/12)°. The other datasets used include the best-track data from the Tropical Cyclone Data Center of the China Meteorological Administration (http://tcdata.typhoon.gov.cn), Climate Forecast System Reanalysis data (http://rda.ucar.edu/datasets/ds093.1/), Climate Forecast System Version 2 data (http://rda.ucar.edu/datasets/ds094.1/), and reanalysis data from the National Centers for Environmental Prediction (NCEP), with a resolution of $0.5^\circ \times 0.5^\circ$.

2.2. *The k-prototype method*

The *k*-prototype method is usually used for clustering or grouping (MacQueen, 1967; Huang, 1997). The landfall position information on all typhoons in this study is a dataset of three main landfall positions are used as clustering criteria to apply on the dataset: the strait between Shandong Peninsula and Liaodong Peninsula (around 38°N); the west coast of the sea area (that is, the China east coast); and the east coast of the sea area (that is, the Korean Peninsula west coast). We calculate the least-squares error between the landfall point and the clustering criteria, and then obtain classified clusters (or groups) of typhoons.

2.3. *Composite diagnosis method*

The composite diagnosis method developed by Rolfson and Smith (1996) and Miao et al. (2015) for synoptic-scale forcing mechanisms is used for TIOEs within the same group in each zone (defined in section 3.3). The formula is as follows:

$$\bar{S}_t(x_i, y_i) = \frac{1}{N} \sum_{n=1}^{N} s_t(x_i, y_i) \,, \tag{1}$$

where $s_t(x_i, y_i)$ is the variable at location (x_i, y_i) and time t, and $\bar{S}_t(x_i, y_i)$ is the composite at location (x_i, y_i). The average of N samples of the variable is calculated at each time and each location in a specific zone, by taking the eddy center as the origin of the moving coordinate, which then forms a composite. More details are given in section 3.3.

3. TIOE statistics in the ECS

3.1. *Classification of typhoons and TIOEs*

There are 13 typhoons that passed over the East China Sea (including the Yellow Sea) during 2005–15 (Fig. 1 and Table 1). Table 1 shows the features of the typhoons and the positions of corresponding TIOEs. According to their tracks and their landfall points, with the *k*-prototype method they can be divided into three groups: Group A (four cases; Fig. 1a; landing points over 38°N): typhoons passing through the central Yellow Sea; Group B (five cases; Fig. 1b; landing points on the western sea coast): typhoons re-entering the sea after landing on continental China; and Group C (four cases; Fig. 1c; landing points on the Korean Peninsula coast): typhoons with paths close to the Korean Peninsula.

To determine whether an ocean eddy is triggered by a typhoon, we track each typhoon for 18 h, in which 6 h are before the typhoon enters into the study sea area and 3 h are after the typhoon has arrived. We then analyze the surface flow

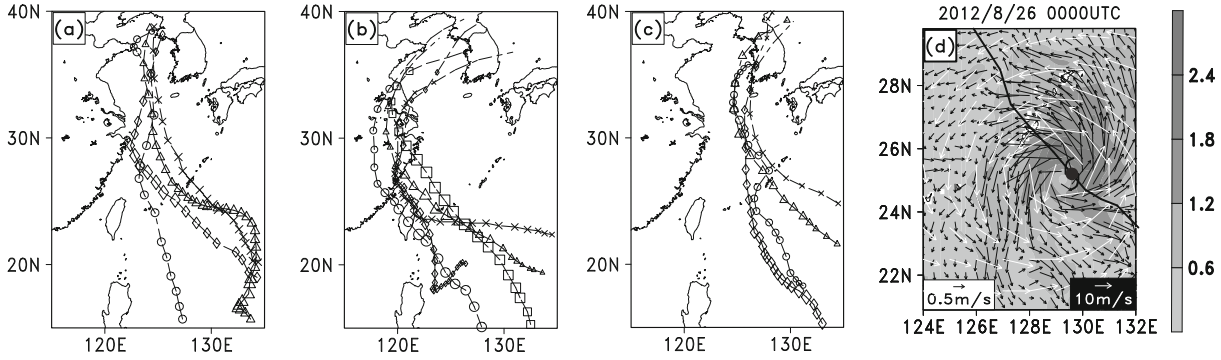

Fig. 1. Typhoon tracks over the ECS during 2005–15: (a) Group A: passing through the central Yellow Sea; (b) Group B: re-entering the sea after landing on continental China; (c) Group C: with paths close to the Korean Peninsula. (d) Typhoon and TIOE (white vectors: typhoon wind; black vectors: sea current; grey spectrum: current intensity; dark dot: typhoon center (129.5°E, 25°N); solid line: typhoon path.

Table 1. Typhoons in the East China Sea (including the Yellow Sea) during 2005–15.

Group/ series No.	Typhoon title-year	Life history (h)	Level of intensity	Max. radius of grade-7 winds (km)	Max. wind speed ($m\ s^{-1}$)	Lowest central pressure (hPa)	TIOE generated
A 1-4	Muifa (2011)	305	Super typhoon	420	55	925	Yes
	Meari (2011)	114	Strong tropical storm	300	30	970	Yes
	Bolaven (2012)	217	Super typhoon	400	52	935	Yes
	Chan-hom (2015)	318	Super typhoon	460	58	925	Yes
B 5-9	Khanun (2005)	152	Strong typhoon	400	50	945	Yes
	Wipha (2007)	101	Super typhoon	420	55	925	Yes
	Kalmaegi (2008)	138	Typhoon	300	35	970	Yes
	Morakot (2009)	186	Typhoon	500	40	955	No
	Matmo (2014)	188	Strong typhoon	320	42	955	Yes
C 10-13	Kalmaegi (2006)	240	Super typhoon	450	55	930	Yes
	Kompasu (2010)	96	Strong typhoon	250	45	955	Yes
	Khanun (2012)	138	Strong tropical storm	180	25	985	Yes
	Nakri (2014)	159	Strong tropical storm	400	25	982	Yes

field of the sea area, and judge whether the selected eddy is indeed triggered by that typhoon (Table 1 and Fig. 1d). As an example, Fig. 1d shows both a typhoon wind circulation (white vectors) and the associated TIOE (black vectors) ocean currents. Their centers are close to each other.

3.2. *Zoning of the study area*

The upper ocean response to each typhoon is not only related to the intensity of the typhoon, track and moving speed, but is also dependent on the geographical environment and physical properties of the sea area. Recent studies suggest that the interaction between the Kuroshio and oceanic eddy impact both the structure of the Kuroshio and the intrusion of the Kuroshio water onto the continental shelf of the East China Sea (Gawarkiewicz et al., 2011; An et al., 2014; Yin, 2014).

As our focus in this study is the features of the TIOEs in the East China Sea and the Yellow Sea, including their interaction with the Kuroshio, we define three zones: Zone I covers a wide deep-water region of the southern part of the Kuroshio in the western Pacific with the Ryukyu Islands inside and a water depth of a few thousand meters; Zone II covers the main part of the Kuroshio; and Zone III covers the shallow water part (less than 100 m) of the northern Kuroshio until the mouth of Bohai Bay. Figure 2 shows the typical paths of the three groups of typhoons and the three zones.

3.3. *Classification of the TIOE composites*

In this study, a TIOE is defined by the circular pattern of the surface current underneath a typhoon. To clearly show the characteristics of the TIOEs' groups in different zones, we composite each TIOE group in each zone.

The basic method of determining the horizontal radius of the composite TIOE is as follows: first, take the eddy center as the origin; according to the basic horizontal scale of the TIOE, 73 HYCOM grids are used in all zonal and meridional directions for all three groups of eddies in Zones I and II. For Zone III, 49 grids are used for Group A and Group C; 25 grids are used for Group B. This is because the TIOEs are smaller in size in Zone III. Equation (1) is then used to obtain the

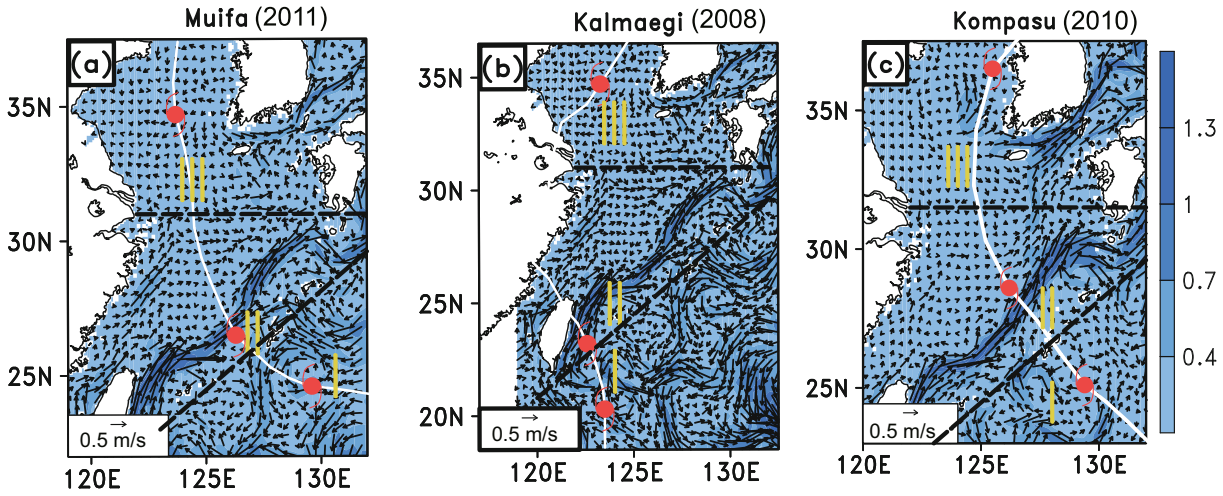

Fig. 2. Tracks of the typhoons in the three groups, along with ocean currents: (a) Muifa (2011), in Group A; (b) Kalmaegi (2008), in Group B; and (c) Kompasu (2010), in Group C. The red dot represents the typical position of the typhoon in the three zones. The vectors show the surface currents (units: m s^{-1}). The black dashed lines indicate the borders of the three zones, and I, II and III indicates their areas.

velocity in each grid, and hence the composite eddy velocity field for each group. The results are shown in Fig. 3.

4. Horizontal features of the TIOEs in each zone

4.1. *Overview of the three TIOE groups*

For the Group A typhoons, whose paths are shown in Fig. 1a, the three zones are shown in Fig. 2a. Taking Typhoon Muifa (2011) as an example, the ocean velocity at 1600 UTC 1 August 2011 is displayed, with each dot indicating the typical location of Muifa (2011) in each zone. For the Group B typhoons, whose paths are shown in Fig. 1b, the three zones where they pass are marked in Fig. 2b. Taking Typhoon Kalmaegi (2008) as an example, the ocean flow at 1600 UTC 14 July 2008 is displayed, with each dot indicating the typical location of Kalmaegi (2008) in each zone. For the Group C typhoons, whose paths are shown in Fig. 1c, the three zones are shown in Fig. 2c. Taking Typhoon Kompasu (2010) is as an example, the flow field at 1600 UTC 28 August 2010 is displayed, with each dot indicating the typical location of Kompasu (2010) as it passes through the zones.

4.2. *Characteristics of the TIOEs in Zone I*

The composite surface current fields of the three TIOE groups in Zone I are shown in Fig. 3. For Group A, the composite TIOE has a strong cyclonic vortex. It moves along with the typhoon toward the northwest, with the northern edge close to the Kuroshio (Figs. 3a and d). At that time, both the typhoon intensity and TIOE intensity are at their peaks. The surface current to the north is westward, which is against the Kuroshio, reversing part of the strong boundary current.

For Group B, the composite TIOE moves westward and usually with high speed in the area. On the eastern side of Taiwan, the southward current on the western rim of the eddy is significantly weakened by the Kuroshio. The current southeastward of the eddy center is strong, showing an obvious deformation in circulation. The eddy is elliptical, elongated in the meridional direction due to the environmental effects (Figs. 3b and e).

For Group C, the track of the composite TIOE is slightly to the east, located south of the Ryukyu Islands. The strong current of the composite TIOE is located on the right-hand side of its moving direction (Fig. 3c). The blocking of the Ryukyu Islands not only affects the eddy intensity, but also induces a small anticyclonic eddy on the western flank of the TIOE (Fig. 3f).

The three groups of TIOEs in Zone I show that strong typhoon winds generally lead to strong TIOE currents, causing asymmetric eddy structures. However, other mechanisms, such as the interaction of ocean systems or a geography, also have an effect: the Group A TIOEs may cause the reversal part of the Kuroshio; the Group B TIOEs are weakened by the Kuroshio and Taiwan Island; and the Group C TIOEs have a reduced current intensity in the presence of the Ryukyu Islands, which may cause an additional eddy to the west.

4.3. *Characteristics of the TIOEs in Zone II*

The composite surface current field of the three TIOE groups in Zone II is shown in Fig. 4. The Group A TIOEs are located in the middle of the study region. With less topographic blockage, these eddies are strong (Figs. 4a and d). When the composite TIOE is near the Kuroshio, its current is stronger than the latter, with the maximum current reaching 1.8 m s^{-1}. As it evolves, the TIOE changes shape: when passing by the Ryukyu Islands, the left-hand side of the eddy is squeezed; after it passes the islands, its original shape is resumed. During its life cycle, the eddy is able to reverse a significant portion of the Kuroshio. When it is close to the east of Taiwan, the eddy could trigger the generation of a small anticyclonic eddy, due to a colligating influence with

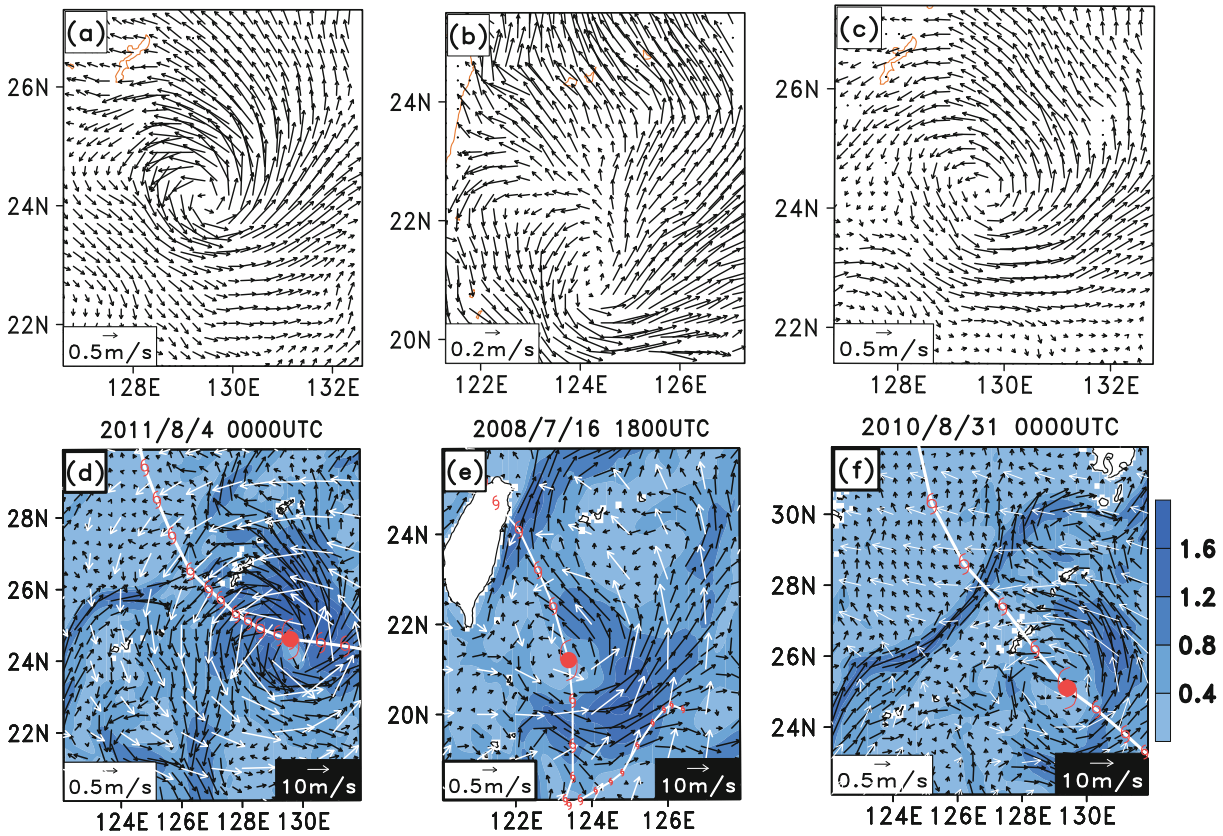

Fig. 3. The surface currents (units: m s^{-1}) with the composite TIOEs in Zone I: (a) Group A; (b) Group B; and (c) Group C. (d) A typical eddy of group A; (e) a typical eddy of group B; (f) a typical eddy of group C. The white arrows are near-sea-surface wind; the white lines with red marks are trajectories of typhoons; and the black arrows show the sea surface current field.

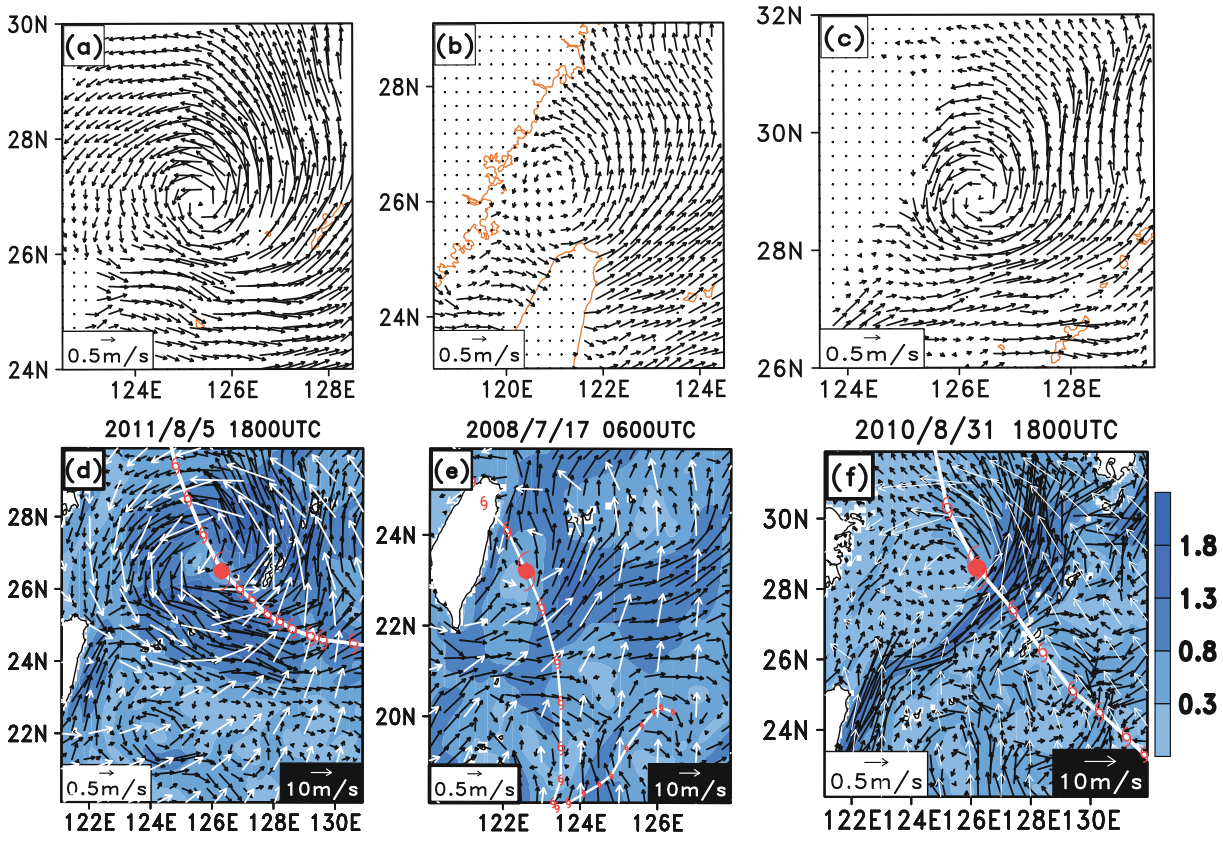

Fig. 4. As in Fig. 3 but in Zone II.

island and the Kuroshio.

When the Group B TIOEs approach the Taiwan Strait and the mainland coast, their intensity is weakened and their positions shifted to the west. The composite eddy is affected by Taiwan Island when moving north. Also, the eddy size is reduced due to the Kuroshio's intensification to the east of the island (Figs. 4b and e). The current on the eddy's western side is significantly weakened, with a maximum speed of only 1.2 m s^{-1}.

By comparison, the paths of the Group C TIOEs are slightly to the east, with a relatively weak intensity and an obvious asymmetry. When the composite eddy enters Zone II, where the Kuroshio and the Ryukyu Islands coexist, the weak current on the western side of the eddy is opposite to the Kuroshio, resulting in zero speed; the current on the eastern side moves in tandem with the Kuroshio, resulting in a broad northward current (Figs. 4c and f). Due to the Kuroshio, the intensity of the eddy is hence affected, with a maximum speed of 1.6 m s^{-1}. After the eddy moves farther north, the strong current in the southeast part of the eddy has a speed similar to that of the Kuroshio; it then joins the main stream, resulting in a broader western boundary current with a speed as high as 1.8 m s^{-1}.

Clearly, the characteristics of the TIOEs are mainly controlled by the intensity of the typhoons. In Zone II, the interaction between the composite TIOE and the Kuroshio is influenced by the strength and location of the TIOE. In addition, the islands and typhoon track are the key factors affecting the state of the eddy, which in turn changes the ocean circulation locally.

4.4. *Characteristics of the TIOEs in Zone III*

The three groups of TIOEs differ significantly in Zone III, due to the shallow water in the area. The Group A TIOEs are strong because of the sustained intensity of the corresponding typhoons. Its composite circulation occupies the whole of the Yellow Sea and is almost symmetric, with the northward component on the eastern side and the southward component on the western side close to 1.6 m s^{-1} (Figs. 5a and d). The Group B typhoons belong to the re-entry type. They are weakened after landfall, and hence the strength of the thus-generated TIOEs is relatively weaker in comparison to that of Group A. Correspondingly, the composite TIOE is smaller in size and moves from southwest toward northeast at a speed of less than 0.7 m s^{-1}, only half that of Group A (Figs. 5b and e), with the flow on the right being stronger than that on the left. The Group C TIOEs have paths slightly toward the east. When moving northward along the west coast of the Korean Peninsula, the composite TIOE is elliptical in form, narrower in the meridional direction. The flow is symmetric, with a maximal speed of 1 m s^{-1} (Figs. 5c and f).

In short, the TIOEs in Zone I are the strongest, which could lead to severe marine disasters. The Zone-II TIOEs have more interaction with the Kuroshio and environmen-

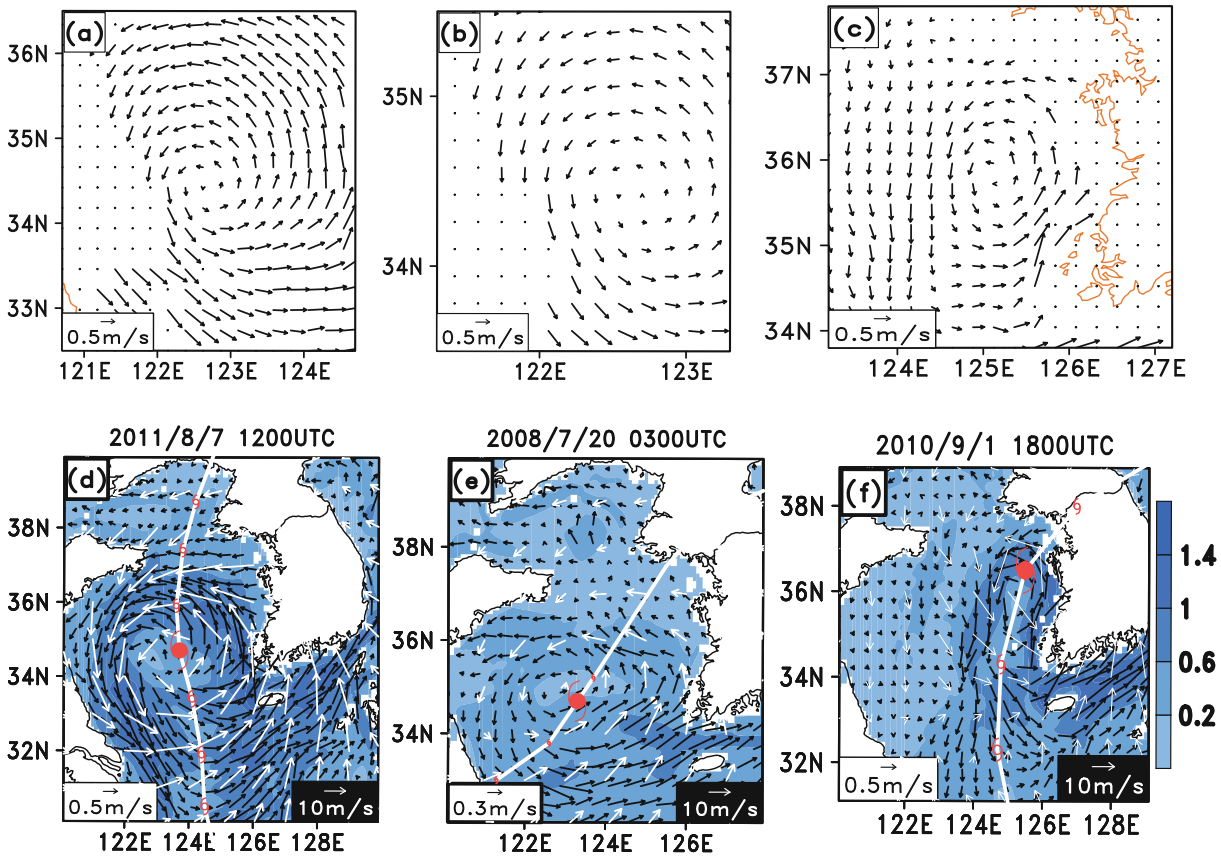

Fig. 5. As in Fig. 3 but in Zone III.

tal topography. So, more deformation appears at the TIOEs and more influence is exerted on the Kuroshio by them. The TIOEs in Zone III are smaller in size and intensity due to the reduced intensity of the typhoon and the influence of the peninsula's topography in the area.

4.5. *Latent and sensible heat fluxes at the air–sea interface*

During the development of a typhoon, a large amount of heat and moisture exchange occurs between the atmosphere and the ocean, which can be represented by the transport of heat flux at the air–sea interface (Jiang et al., 2012). Out of all the heat fluxes thus exchanged, the heat transport from the ocean mixed layer accounts for 85% (Price, 1981).

The asymmetric structure of the typhoon will greatly affect the heat flux distributions. Statistically, the area with strong winds or currents is to the right of the typhoon track in Zone I, in the northeast of the typhoon circulation in Zone II, and to the southeast of the track in Zone III. Analysis also shows that the area with maximal latent heat flux coincides with the area with strong TIOE currents. Table 2 shows the statistics of heat flux in those three zones for all the typhoons/TIOEs of concern. It shows the latent heat is larger in Zone I and Zone II than that in Zone III. This is probably related to the abundant moisture at lower latitudes and/or stronger currents in these two zones. The strong TIOE currents contribute substantially to the positive latent heat flux at the air–sea interface, which forms a positive feedback loop in the typhoon's development. Compared to the latent heat flux, the sensible heat flux is much smaller, and has little correlation with strong currents.

5. Vertical structure of a typical TIOE and its associated energy transfer

5.1. *Case selection*

Of the TIOEs in the three different groups, the TIOEs of Group C experience significant deformation, while the TIOEs of Group B differ conspicuously in intensity from zone to zone. The TIOEs in these two groups often display deformation, and even incomplete eddy structures. We hence select the eddy induced by Typhoon Muifa (2011) of Group A as a typical example to analyze the TIOE vertical structure and energy transport.

5.2. *SST changes*

Typhoons are a low-pressure system with closed circulation and strong cyclonic winds. Based on Ekman theory, the direction of surface currents in the Northern Hemisphere is at 45° to the right of surface winds. Therefore, the surface water of the Muifa-induced TIOE flows outward from the center. The strong divergent flow of the TIOE causes remarkable local upwelling, which results in a decrease in SST (Fig. 6). At 1600 UTC 3 August, a significant decrease (1°C–6°C) in SST occurs in the east of the TIOE (Fig. 6a). At 0400 UTC 5 August, Muifa (2011) moves northwestward and enters Zone II, leaving a cold wake behind (Fig. 6b). The

Table 2. Latent and sensible heat fluxes (units: W m^{-2}) in the area of strong currents within the TIOE.

	Average latent heat flux (W m^{-2})			Average sensible heat flux (W m^{-2})		
TIOE	Zone I	Zone II	Zone III	Zone I	Zone II	Zone III
All TIOES	392.7	362.6	126.4	−3.4	−19.5	−16
Group A	493.0	343.8	314.5	−16.5	−50.2	−35.2
Group B	343.8	341.6	116.2	5.0	−1.4	0.4
Group C	314.5	321.5	170.0	1.5	−3.5	−18.5

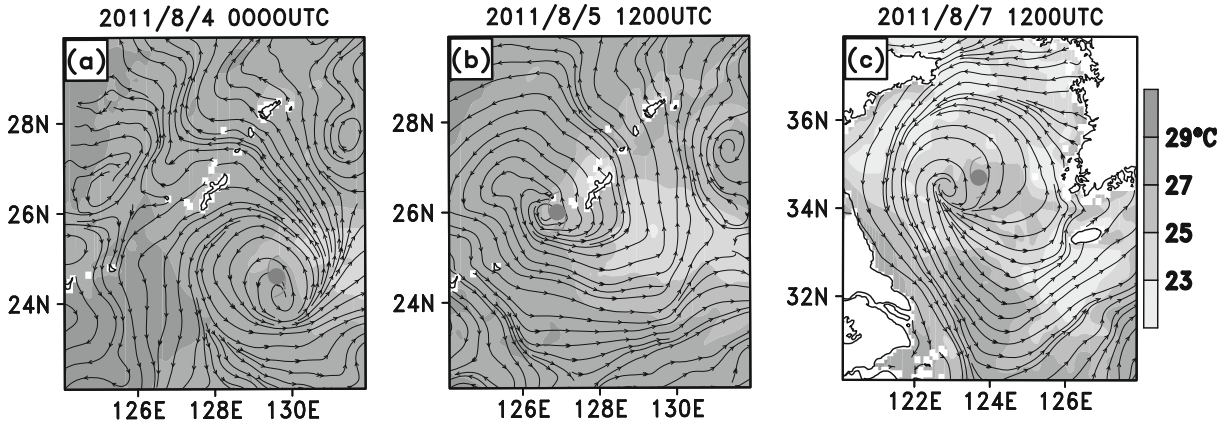

Fig. 6. The SST (units: °C) with the TIOE generated by Typhoon Muifa (2011) in the three zones (a) at 1600 UTC 3 August 2011 in Zone I, (b) at 0400 UTC 5 August in Zone II, and (c) at 0400 UTC 7 August in Zone III. The dark dot indicates Typhoon Muifa (2011)'s position. The grey bar shows the SST field and the streamlines are the sea surface current field.

cold area is collocated with the divergent area, with a divergent flow more significant to the right of the track, which is a more favorable condition for upwelling to the right of the TIOE and results in an asymmetric SST distribution. Figure 6c shows the SST distribution around the TIOE after it enters Zone III. Because Zone III is at higher latitude, the ambient SST is much cooler. The divergent flow generated by the TIOE further cools the water in the neighborhood. The resulting SST ranges from 20°C to 27°C, which is much colder than that in Zone I (31°C) and Zone II (30°C).

5.3. *Sectional temperature distribution*

According to the SST distribution in the TIOE area in Fig. 6, we select the cold center on the right of the track in each zone to analyze the vertical temperature profile. As seen in Fig. 7, the cold center (marked as a triangle) corresponds to an obvious cold tongue underneath the mixed layer, indicating a deep upwelling. In Zone I, the contour of the temper-

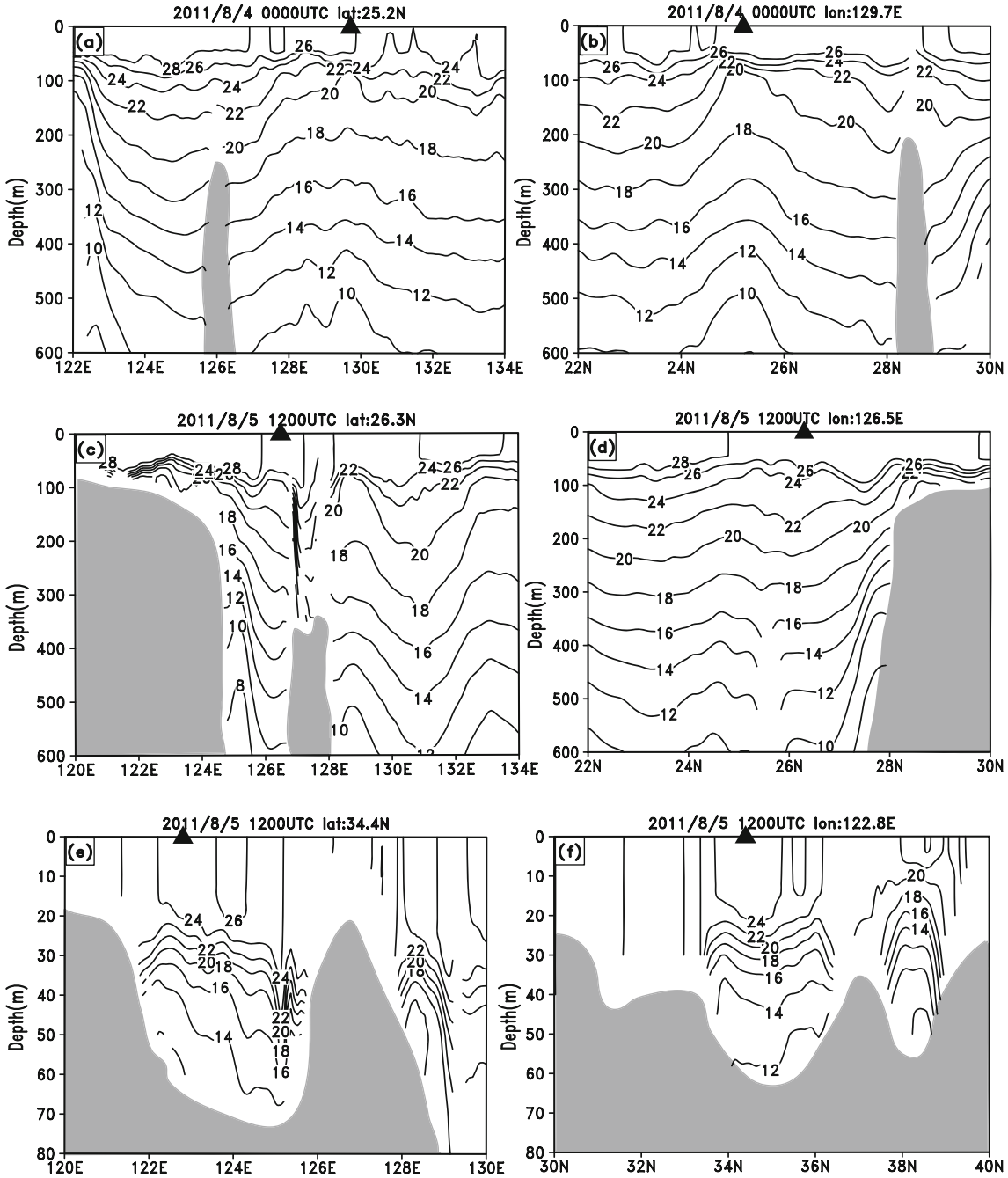

Fig. 7. Vertical cross section of upper-ocean temperature through the cold center of the TIOE generated by Typhoon Muifa (2011) (units: °C). Left-hand panels: along a fixed latitude; right-hand panels: along a fixed longitude. (a, b) Zone I; (c, d) Zone II, and (e, f) Zone III. The black triangle indicates the SST cold-center position. The shaded parts are the sea bottom and topography.

ature near the cold center bulges up, extending through 100 m (Figs. 7a and b). This feature is clearer in a latitudinal vertical cross section (Fig. 7b) than in a longitudinal one (Fig. 7a). Figure 7b clearly shows that the cold tongue is as deep as 600 m, while the thermocline is around 100 m near the surface. Note there are many islands in Zone II, which may also cause the topographic-induced upwelling. This is identifiable in Fig. 7c (to the left of the cold center) and Fig. 7d (to the right of the cold center). The bulging of the contour is not as apparent as that in Zone I, indicating a weaker upwelling. This suggests that the islands may have a crucial impact on the distribution of the physical properties of the eddy. Zone III is narrow and shallow, with a depth only down to 80 m. The upwelling in this zone is very weak, and the thermocline is at about 30–50 m below the surface.

5.4. *Sectional salinity distribution*

Figure 8 shows the longitudinal vertical distribution of salinity at the cold center. It reveals that all the cold centers in different zones correspond to a mixed layer of salinity near the surface, and the typhoon circulation and the associated TIOE increase the depth of the layer. Simultaneously, significant salinity fluctuations can be noticed below 300 m in Zone I and Zone II (Figs. 8a and b), corresponding to the upwelling of the deep water. There is also an upwelling associated with the terrain in Zone II, which can be seen near the grey shaded area on the right in Fig. 8b. As for Zone III, the depth of the water is only 80 m (Fig. 8c), and the halocline is at about 60–20 m. Therefore, the cold wake of a typhoon is also a wake of low salinity.

5.5. *Sectional distribution of the TIOE flow*

Figure 9 shows the vertical cross section distributions of the horizontal flow and the kinetic energy associated with the TIOE. The black solid dot in Fig. 9 indicates the center of eddy.

The formula used to calculate the kinetic energy K is

$$K = \rho(u^2 + v^2)/2\,, \tag{2}$$

where ρ is the density; and u and v (units: m s^{-1}) are the horizontal velocity components.

According to Fig. 9, a common feature of the horizontal flow of the TIOE at different levels in different zones is its asymmetric structure. In Zone I, the horizontal flows in the east (Fig. 9a) and north (Fig. 9b) are stronger than those in the west and south. The corresponding kinetic energy distribution (contours) shows a consistent pattern (Figs. 3a and 6a). The intensity of the horizontal flow decays quickly with depth, but the maximal depth of the flow reaches as deep as 700 m. The dominant feature of the TIOE in Zone II is the penetration depth of the horizontal circulation (Figs. 9c and d). In the west and north, the contour of 0.1 J reaches as deep as 500 m, compared with 100 m in Zone I. This is probably related to the impacts from the Kuroshio and the Ryukyu Islands. In Zone III, the horizontal flow associated with the TIOE is noticeable throughout the entire water column (80 m) (Figs. 9e and f), and the kinetic energy contour of 0.1 J is at the depth of 40 m. One of the special aspects in Zone III is the reversal of horizontal flow in the east and north at about 30 m. This may be related to the bottom Ekman layer, but more research is needed before a conclusion is made.

5.6. *TIOE energy transport*

When a TIOE moves in the ocean, strong kinetic energy is transported downward. In this section, we analyze the kinetic energy transport and its evolution around the center of the eddy, as well as in the area with strong currents.

Figure 10 shows the temporal evolutions of kinetic energy at the TIOE center (Figs. 10a, c and e) and in the strong current areas (Figs. 10b, d and f) in different zones. In Zone I, the maximal kinetic energy is about 2.5 J at both the eddy center and in the strong currents area. It takes 12 h for the 0.4 J kinetic energy contour at the eddy enter to reach 60 m, while it only takes 9 h for the same kinetic energy contour to reach about 80 m in the strong current area (Figs. 10a and b). In Zone II, the maximal kinetic energy is about 1.4 J at the eddy center, but 3.3 J in the strong currents area. It takes 15 h for the 0.2 J kinetic energy contour at the eddy center to reach 60 m, but in the strong currents area it takes only 5 h for the 0.9 J contour to reach 90 m (Figs. 10c and d). In Zone III, the maximal kinetic energy is about 0.7 J near the surface. Within the same period, the 0.1 J kinetic energy contour at the eddy center reaches 22 m, while it penetrates more than 30 m in the strong currents area (Figs. 10e and f).

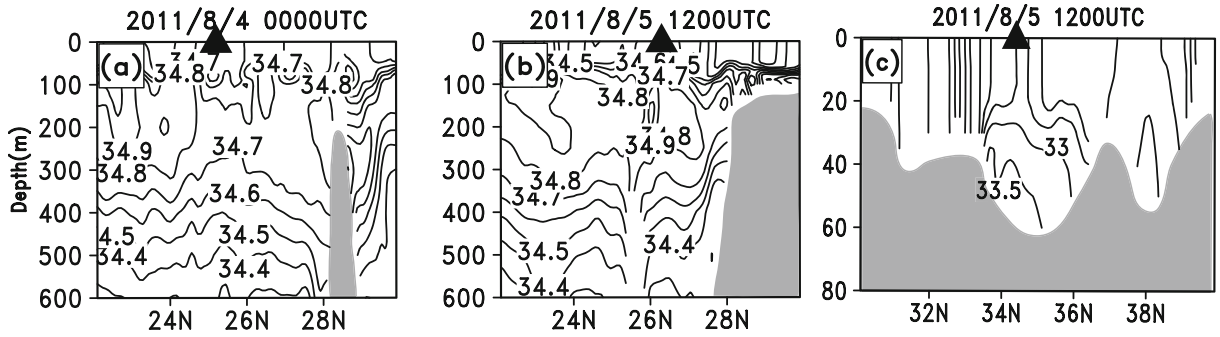

Fig. 8. Vertical longitudinal cross section distribution of salinity at the cold center of the TIOE with Muifa (2011) (units: psu): (a) Zone I; (b) Zone II; (c) Zone III. The black triangle represents the position of the cold center. The shaded parts are the sea bottom and topography.

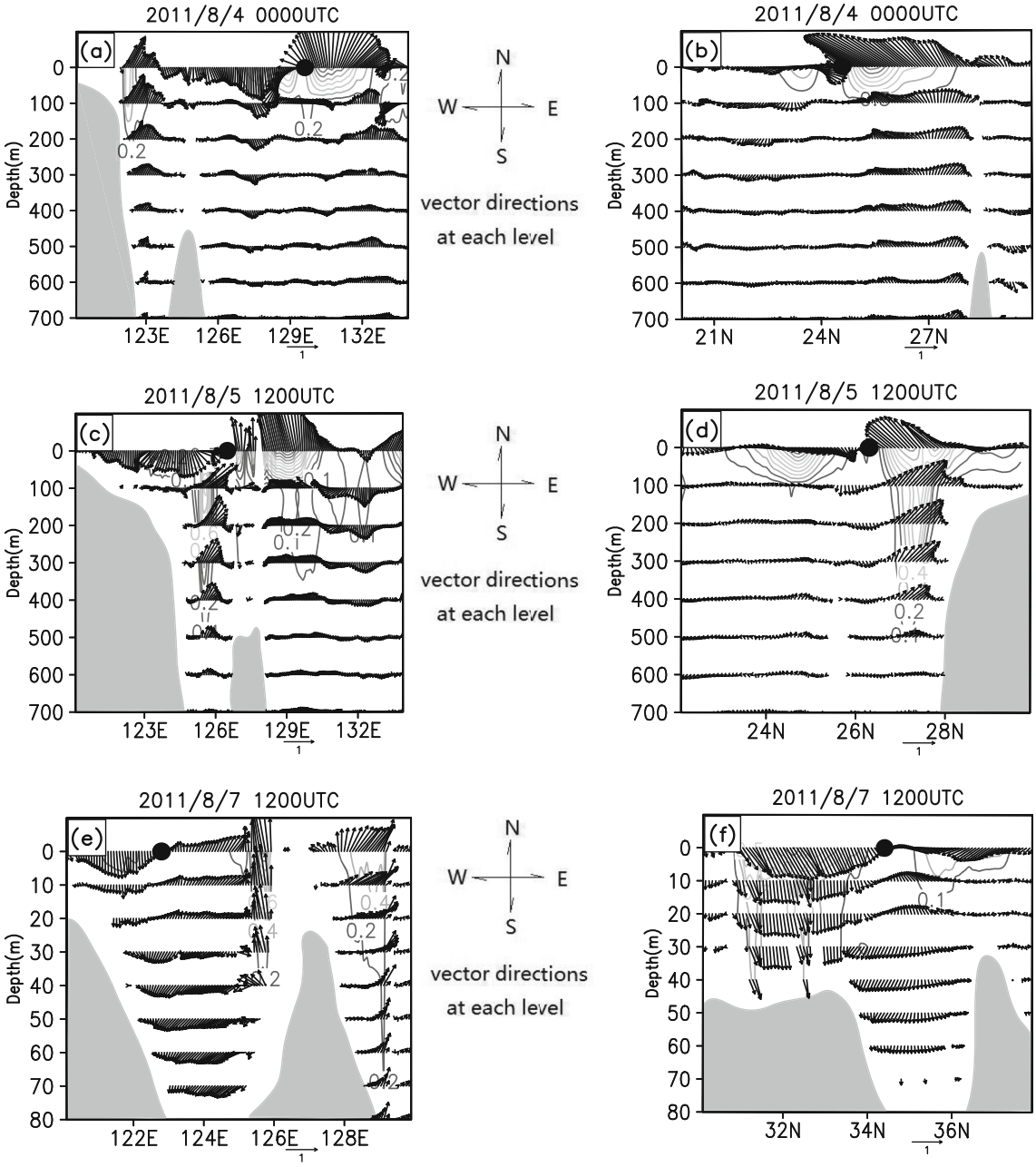

Fig. 9. Vertical cross section distributions of the horizontal current vector and kinetic energy in the TIOE of Muifa (2011) (units: J). The section passes through the center of the eddy. (a, c, e) The vertical latitudinal and (b, d, f) the vertical longitudinal distributions. (a, b) Zone I; (c, d) Zone II; (e, f) Zone III. The black dot represents the center of the TIOE. The shaded parts are the sea bottom and topography. The vectors are horizontal currents, the contours are kinetic energy (unit: J).

In general, the kinetic energy (larger than 0.2 J) associated with a strong eddy flow can only reach halfway along the TIOE's vertical extent. The strong currents of the TIOE generate a greater, faster, and deeper energy transfer than at the center of the TIOE.

6. Conclusion

In this study, 13 TIOEs in the East China Sea (including the Yellow Sea) are analyzed. With the *k*-prototype method, they were divided into three groups by tracks and landfall positions of typhoons: Group A, with typhoons passing through the central Yellow Sea; Group B, with typhoons re-entering the sea from the western Yellow Sea after landing on continental China; and Group C, with typhoons along the eastern Yellow Sea and close to the Korean Peninsula. Meanwhile, the study area is also divided into three zones according to water depth and where the Kuroshio appears. The characteristics of the TIOEs in the three groups and zones are compared. The following is a summary of the main results:

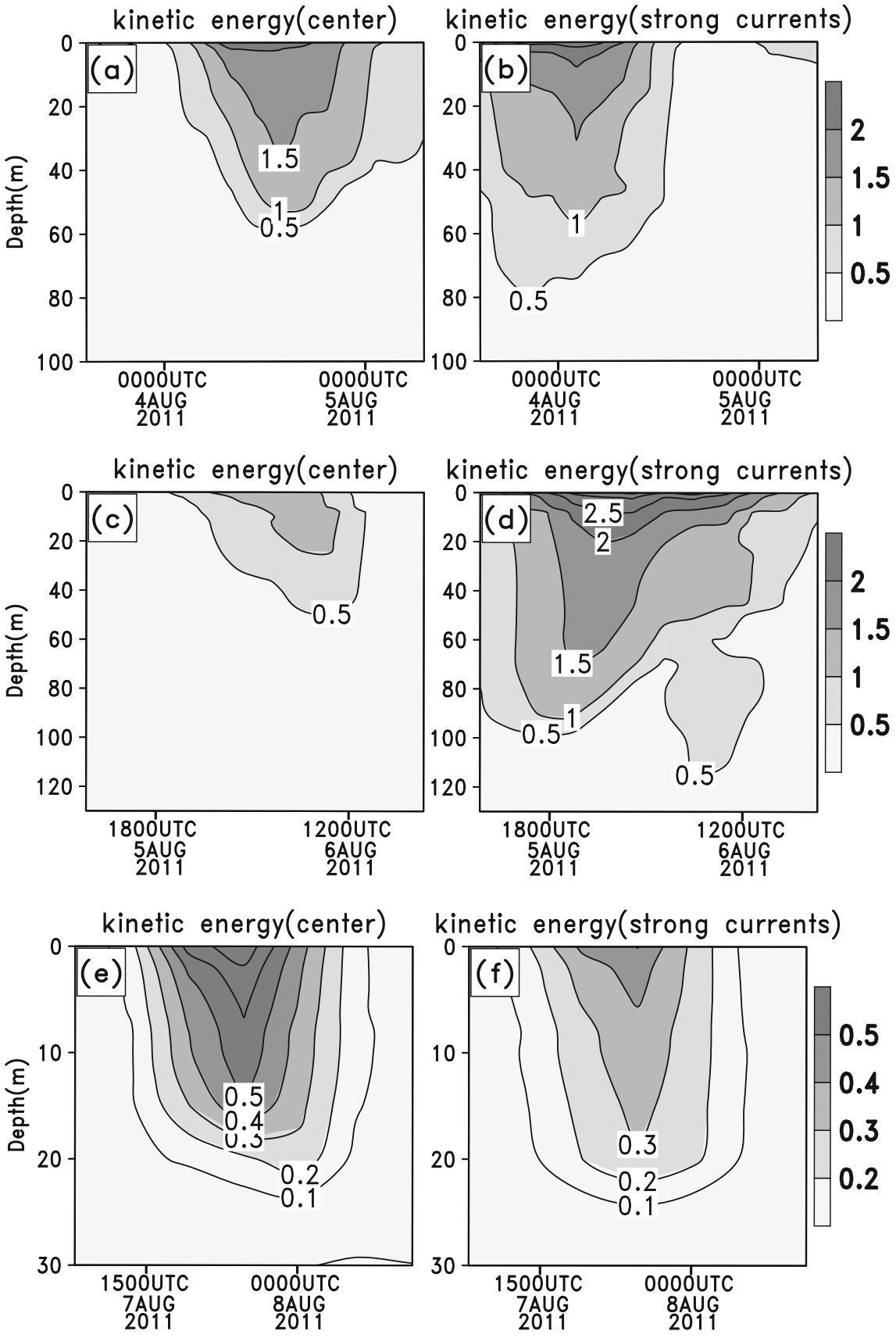

Fig. 10. Evolution of the kinetic energy transport at the center and the strong currents of the TIOE (unit: J) in (a, b) Zone I, (c, d) Zone II and (e, f) Zone III.

(1) All the TIOEs are asymmetric in structure. The area with strong typhoon winds coincide with the area with strong TIOE currents. In Zone I, the TIOEs in Group A are the strongest, causing some countercurrents in the Kuroshio. The TIOEs in Group B are close to Taiwan, deforming and decaying due to the presence of the Kuroshio and Taiwan. The TIOEs in Group C are significantly influenced by the Ryukyu Islands; they deform and may even induce new eddies. In addition, the strong currents associated with the Group C TIOEs could be superimposed on the Kuroshio, resulting in an enhanced stream in the east of the western boundary current. In Zone III, due to the strong Group A TIOEs, almost the entire Yellow Sea is occupied by its circulation, which may lead to disastrous winds and waves. The TIOEs in Group B and C are relatively weak and deform easily, since they are significantly impacted by the land or islands to which they are close.

(2) TIOEs play an important role in transporting heat at the air–sea interface. Particularly, the asymmetric structure of TIOEs exerts critical influences on the heat flux distribution and intensity. We have seen that the maximal latent heat flux is proportional to the area with strong TIOE currents, forming a positive feedback loop in the development of typhoons. Zone I and Zone II are at low latitudes, where the moisture vapor is abundant and the TIOEs are stronger. The latent heat flux is hence large in comparison to that in Zone III. Compared with the latent heat flux, the sensible heat flux has much smaller values and has little correlation with strong currents.

(3) Typically, in Zone I, the major cooling area is to the east of the TIOE. In Zone II, a cold wake forms following the track of the typhoon. In Zone III, because of the higher latitude and colder SSTs, cold centers correspond to the divergent areas and surround the center of the TIOE. The strong divergence favors an upwelling-induced cooling, and a low salinity condition. A deepened mixed layer can be found underneath the cold SST center, and the layer with colder and fresher water due to the strong upwelling is under the mixed layer. The vertical structure of a typical TIOE shows that the intensity of the upwelling within the TIOE is proportional to the water depth in each zone, but its magnitude is weaker than the upwelling resulting from the coastal topography nearby.

(4) Vertical cross section maps of the horizontal flow and energy transport in a typically strong TIOE reveal that the surface flow decays quickly with depth. The penetration depth in Zone I and Zone II is about 700 m, and can reach the bottom (about 80 m) in Zone III. A conspicuous feature is the reversal of the horizontal flow at about 30 m in Zone III. In general, the kinetic energy (larger than 0.2 J) under a strong TIOE flow can only reach halfway along the TIOE's vertical extent. The strong currents of the TIOE generate a greater, faster, and deeper energy transfer than at the center of the TIOE.

Acknowledgements. Thanks are extended to the China Meteorological Administration (http://tcdata.typhoon.gov.cn), NCEP (http://rda.ucar.edu/datasets/ds093.1/, http://rda.ucar.edu/datasets/ds094.1/), and the HYCOM Consortium (http://hycom.org/dataserver/), for providing the datasets. This work was supported by the National Natural Science Foundation of China (Grant Nos. 41276033 and 41276032), the Jiangsu Science and Technology Support Project (Grant No. BE2014729), and a project funded by the Priority Academic Program Development of Jiangsu Higher Education Institutions. the 2015 Jiangsu Program for Innovation Research and Entrepreneurship Groups, and the National Program on Global Change and Air-Sea Interaction (GASI-IPOVAI-06).

REFERENCES

An, Y. Z, Y. L. Wang, and R. Zhang, 2014: Upper ocean temperature and salinity structure response to typhoon. *Second Symposium on Disaster Risk Analysis and Management in Chinese Littoral Regions*, China Disaster Defense Association risk analysis Specialized Committee, Haikou, 44–48. (in Chinese with English abstract)

Black, P. G., 1983: temperature changes induced by tropical cyclones. PhD. dissertation, The Ocean Pennsylvania State University, 1487 pp.

Chen, D. K., X. T. Lei, W. Wang, G. H. Wang, G. J. Han, and L. Zhou, 2013: Upper ocean response and feedback mechanisms to typhoon. *Advances in Earth Science*, **28**(10), 1077–1086, https://doi.org/10.11867/j.issn.1001-8166.2013.10.1077. (in Chinese with English abstract)

Domingues, R., and Coauthors, 2015: Upper ocean response to Hurricane Gonzalo (2014): Salinity effects revealed by targeted and sustained underwater glider observations. *Geophys. Res. Lett.*, **42**(17), 7131–7138, https://doi.org/10.1002/2015GL065378.

Emanuel, K. A., 1999: Thermodynamic control of hurricane intensity. *Nature*, **401**, 665–669, https://doi.org/10.1038/44326.

Gawarkiewicz, G., and Coauthors, 2011: Circulation and intrusions northeast of Taiwan: Chasing and predicting uncertainty in the cold dome. *Oceanography*, **24**(4), 110–121, https://doi.org/10.5670/oceanog.2011.99.

Huang, Z. X., 1997: A fast clustering algorithm to cluster very large categorical data sets in data mining. *Proceedings of the SIGMOD Workshop on Research Issues on Data Mining and Knowledge Discovery*, Arizona, ACM Press, 1–8.

Jiang, D., F. Huang, G. H. Hao, and W. H. Lv, 2012: The characteristics of air-sea heat flux exchange during the generation and development of the local typhoon over the south China sea. *Journal of Tropical Meteorology*, **28**(6), 888–896, https://doi.org/10.3969/j.issn.1004-4965.2012.06.010. (in Chinese with English abstract)

Leipper, D. F., 1967: Observed ocean conditions and Hurricane Hilda, 1964. *J. Atmos. Sci.*, **24**(2), 182–186, https://doi.org/10.1175/1520-0469(1967)024<0182:OOCAHH>2.0.CO;2.

Li, Y. X., 2015: Typhoons' effects on ocean cyclonic eddies in the North Western Pacific. M.S. thesis, University of Science and Technology of China. (in Chinese with English abstract)

Lin, P. F., 2005: Statistical analyses on mesoscale eddies in the South China Sea and the Northwest Pacific. M.S. thesis, Institute of Oceanology, University of Chinese Academy of Sciences. (in Chinese with English abstract)

Liu, G. P., and J. Y. Hu, 2009: Response of the mesoscale eddies to tropical cyclones in the South China Sea: A case study. *Journal of Oceanography in Taiwan Strait*, **28**(3), 308–315, https://doi.org/10.3969/j.issn.1000-8160.2009.03.002. (in Chinese with English abstract)

Liu, Z. H., J. P. Xu, C. H. Sun, and X. F. Wu, 2014: An upper ocean response to Typhoon Bolaven analyzed with Argo profiling floats. *Acta Oceanologica Sinica*, **33**(11), 90–101, https://doi.org/10.1007/s13131-014-0558-7.

Liu, Z. H., J. P. Xu, B. K. Zhu, C. K. Sun, and L. F. Zhang, 2007: The upper ocean response to tropical cyclones in the northwestern Pacific analyzed with Argo data. *Chinese Journal of Oceanology and Limnology*, **25**(2), 123–131, https://doi.org/10.1007/s00343-007-0123-8.

Ma, J., H. M. Xu, and C. M. Dong, 2014: Atmospheric Response to mesoscale oceanic eddies over the Kuroshio extension: Case analyses of warm and cold eddies in winter. *Chinese Journal of Atmospheric Sciences*, **38**(3), 438–452, https://doi.org/10.3878/j.issn.1006-9895.2013.13151. (in Chinese with English abstract)

MacQueen, J., 1967: Some methods for classification and analysis of multivariate observations. *Proc. 5th Symposium on Mathematics & Statistical Probability*, Berkeley, University of California, 281–296.

Miao, C. S., P. Song, J. H. Wang, and D. Niu, 2015: Comparative study of impact factors of the yellow river cyclones over the Bohai Sea in spring and summer. *Meteorological Monthly*, **41**(9), 1068–1078, https://doi.org/10.7519/j.issn.1000-0526.2015.08.003. (in Chinese with English abstract)

Monaldo, F. M., T. D. Sikora, S. M. Babin, and R. E. Sterner, 1996: Satellite imagery of sea surface temperature cooling in the wake of Hurricane Edouard (1996). *Mon. Wea. Rev*., **125**(10), 2716–2721, https://doi.org/10.1175/1520-0493(1997)125<2716:SIOSST>2.0.CO;2.

Nam, S. H., D. J. Kim, and W. M. Moon, 2012: Observed impact of mesoscale circulation on oceanic response to Typhoon Man-Yi (2007). *Ocean Dynamics*, **62**(1), 1–12, https://doi.org/10.1007/s10236-011-0490-8.

Nencioli, F., C. M. Dong, T. Dickey, L. Washburn, and J. C. McWilliams, 2010: A vector geometry–based eddy detection algorithm and its application to a high-resolution numerical model product and high-frequency radar surface velocities in the southern California bight. *J. Atmos. Oceanic Technol*., **27**, 564–579, https://doi.org/10.1175/2009JTECHO725.1.

Price, J. F., 1981: Upper ocean response to a hurricane. *J. Phys. Oceanogr*., **11**, 153–175, https://doi.org/10.1175/1520-0485(1981)011<0153:UORTAH>2.0.CO;2.

Qin, D. D., J. H. Wang, Y. Liu, and C. M. Dong, 2015: Eddy analysis in the Eastern China Sea using altimetry data. *Frontiers of Earth Science*, **9**, 709–721, https://doi.org/10.1007/s11707-015-0542-3.

Rolfson, D. M., and P. J. Smith, 1996: A composite diagnosis of synoptic-scale extratropical cyclone development over the United States. *Mon. Wea. Rev*., **124**(6), 1084–1099, https://doi.org/10.1175/1520-0493(1996)124<1084:ACDOSS>2.0.CO;2.

Shang, X. D., C. Xu, G. Y. Chen, and S. M. Lian, 2013: Review on mechanical energy of ocean mesoscale eddies and associated energy sources and sinks. *Journal of Tropical Oceanography*, **32**(2), 24–36, https://doi.org/10.3969/j.issn.1009-5470.2013.02.003. (in Chinese with English abstract)

Shay, L. K., 2010: Air-sea interactions in tropical cyclones. *Global Perspectives on Tropical Cyclones*, J. C. L. Chan and J. D. Kepert, Eds., World Scientific Publishing Company, 93–131.

Sun, L., Y. X. Li, Y. J. Yang, Q. Y. Wu, X. T. Chen, Q. Y. Li, Y. B. Li, and T. Xian, 2014: Effects of super typhoons on cyclonic ocean eddies in the western North Pacific: A satellite data-based evaluation between 2000 and 2008. *J. Geophys. Res*., **119**, 5585–5598, https://doi.org/10.1002/2013JC009575.

Sun, L., Y. J. Yang, T. Xian, Y. Wang, and Y. F. Fu, 2012: Ocean responses to typhoon Namtheun explored with Argo floats and multiplatform satellites. *Atoms.-Ocean*, **50**(5), 15–26, https://doi.org/10.1080/07055900.2012.742420.

Tanajura, C. A. S, A. N. Santana, D. Mignac, L. N. Lima, K. Belyaev, and J. P. Xie, 2014: The REMO ocean data assimilation system into HYCOM (RODAS_H): General description and preliminary results. *Atmospheric And Oceanic Science Letters*, **7**(5), 464–470, https://doi.org/10.3878/j.issn.1674-2834.14.0011.

Tsai, Y. L., C. S. Chern, S. Jan, and J. Wang, 2013: Numerical study of cold dome variability induced by typhoon Morakot (2009) off northeastern Taiwan. *J. Mar. Res*., **71**, 109–131, https://doi.org/10.1357/002224013807343434.

Wentz, F. J., C. Gentemann, D. Smith, and D. Chelton, 2000: Satellite measurements of sea surface temperature through clouds. *Science*, **288**, 847–850, https://doi.org/10.1126/science.288.5467.847.

Yang, G., F. Wang, Y. L. Li, and P. F. Lin, 2013: Mesoscale eddies in the northwestern subtropical Pacific Ocean: Statistical characteristics and three-dimensional structures. *J. Geophys. Res*., **118**(4), 1906–1925, https://doi.org/10.1002/jgrc.20164.

Yang, Y. J., Y. F. Fu, L. Sun, P. Liu, and S. Feng, 2010: Responses of the upper ocean to Typhoon Tingting observed from multiplatform satellites and Argo float. *Journal of University of Science and Technology of China*, **40**(1), 1–7, https://doi.org/10.3969/j.issn.0253-2778.2010.01.001. (in Chinese with English abstract)

Yang, Y. J., T. Xian, L. Sun, Y. F. Fu, and S. P. Xun, 2012: Impacts of sequential typhoons on sea surface temperature and sea surface height in September 2008. *Acta Oceanologica Sinica*, **34**(1), 71–78. (in Chinese with English abstract)

Yin, Y. Q., 2014: A study on the impact of mesoscale eddies on Kuroshio intrusion variations northeast of Taiwan and its underlying mechanism. PhD dissertation, Ocean University of China. (in Chinese with English abstract)

Zhang, X. S., Z. F. Wang, B. Wang, K. J. Wu, G. J. Han, G. J. Han, and W. Li, 2014: A numerical estimation of the impact of Stokes drift on upper ocean temperature. *Acta Oceanologica Sinica*, **33**(7), 48–55, https://doi.org/10.1007/s13131-014-0507-5.

Zheng, Z. W., C. R. Ho, Q. N. Zheng, Y. T. Lo, N. J. Kuo, and G. Gopalakrishnan, 2010: Effects of preexisting cyclonic eddies on upper ocean responses to Category 5 typhoons in the western North Pacific. *J. Geophys. Res*., **115**, C09013, https://doi.org/10.1029/2009JC005562.